IOP Publishing Superconductor Science and Technology
Supercond. Sci. Technol. 31 (2018) 045006 (10pp) https://doi.org/10.1088/1361-6668/aaadf6

Significance of out-of-plane electronic contributions in Bi-cuprates studied by resonant photoelectron spectroscopy at the Cu2p edge

Christoph Janowitz[1] and **Dieter Schmeißer**[2]

[1] Institut für Physik, Humboldt-Universität zu Berlin, Newtonstr. 15, 12489 Berlin, Germany
[2] Angewandte Physik-Sensorik, BTU Cottbus-Senftenberg, Konrad-Wachsmann-Allee 17, 03046 Cottbus, Germany

E-mail: janowitz@physik.hu-berlin.de

Received 27 November 2017, revised 30 January 2018
Accepted for publication 8 February 2018
Published 6 March 2018

Abstract

In high-temperature superconductors with a layered crystal structure, the copper–oxygen planes are commonly considered to dominate the electronic properties around the Fermi energy. As a consequence, out-of-plane contributions are often neglected in the description of these materials. Here we report on a resonant photoemission study of $Pb_{0,4}Bi_{1,6}Sr_{2,0}CaCu_2O_8$ ((Pb, Bi)-2212) and $Pb_{0,6}Bi_{1,4}Sr_{1.5}La_{0.5}CuO_6$ ((Pb, Bi)-2201)) single crystals to unravel the resonant decay mechanisms at the Cu2p absorption edge. We find evidence for a pronounced polarization dependence caused by two different Auger processes for in-plane and out-of-plane orientations. We deduce that the lowest energy valence state—which is involved in the two Auger processes—consists of three-dimensional contributions by admixed out-of-plane Sr, Bi, and O2p states. It also suggests that the doping-induced charge density is dynamic, fluctuating within the Cu–O plane, and spills out perpendicular to it. This suggests that out-of-plane electronic degrees of freedom should be included in future consistent theoretical models of these materials.

Keywords: synchrotron radiation, polarization dependence, 3D hole doping, superconductor

(Some figures may appear in colour only in the online journal)

Introduction

In high-T_c superconducting cuprates/oxides there is a long-lasting debate about the role of three-dimensional (3D) features, in particular the influence of the apical oxygen (O_{api}) atom [1]. Since the discovery of high-temperature superconductivity [2], the question of whether out-of-plane orbitals and/or atoms play a decisive role has been mostly discarded. Prototypical models for the CuO_2 layers were elaborated, such as effective single-band [3] and two-band models [4]. However, according to the Mermin–Wagner theorem [5] they cannot be reconciled with a long-range superconducting order—besides a topological order below the Kosterlitz–Thouless transition temperature [6]. Strictly two-dimensional (2D) models have been questioned [7–9] as they are limited to O2p and Cu3d states only. They are replaced by more sophisticated models, including at least the states of the apical oxygen atom as an out-of-plane contribution [10–16], and it is usually argued that inter-plane coupling will enhance the superconducting state. Strong correlation effects inherent to models with reduced dimensionality, such as the 2D Hubbard model, are outside the scope of this publication.

Experimental verification of the non-planar contributions has been carried out in various studies (e.g. the review by Feiner *et al* [16]), including energy-loss, x-ray absorption, Raman, and two-photon pump-probe experiments, to name a few. Here we employ resonant photoelectron spectroscopy (resPES), a technique which has element and orbital selective information about the electronic structure in the valence band (VB) and conduction band (CB) states [17, 18]. Our

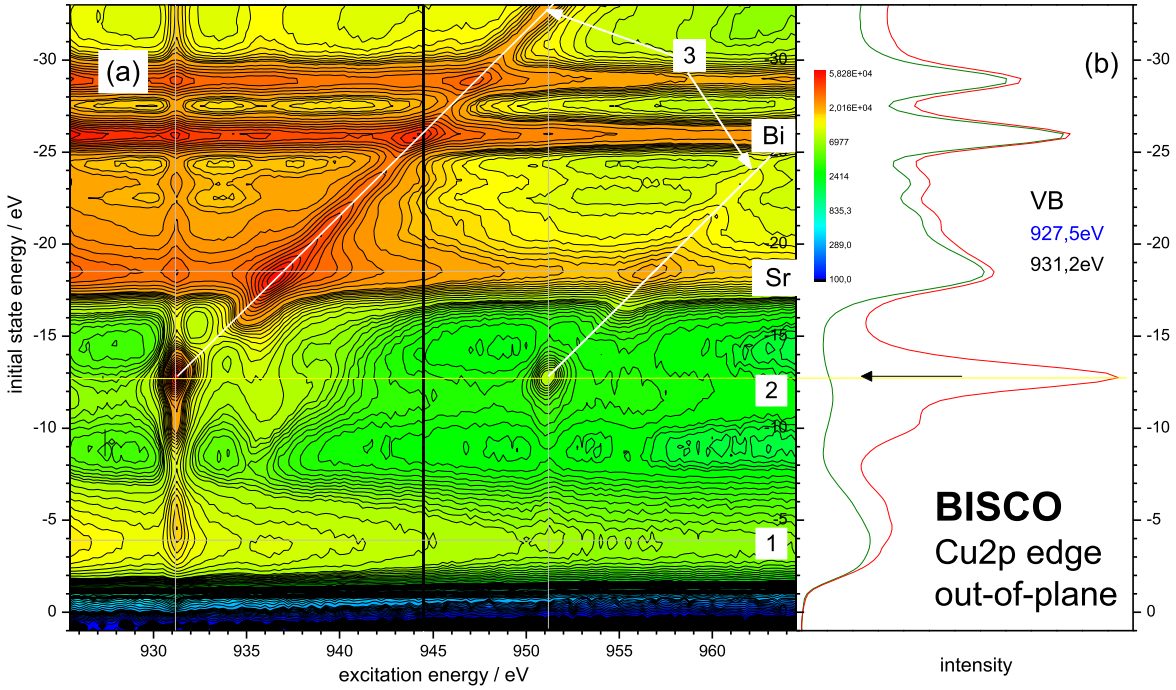

Figure 1. (a) The resPES profile of ((Pb, Bi)-2212) at the Cu2p edge, recorded at RT in out-of-plane polarization. The data have been recorded in separate runs and are stitched together at the black line. The numbers on the right denote: photoemission signal of the VB (1); $Cu3d^8$ satellite (2); Cu-LMM Auger process (3). (b) The VB data recorded before (927.5 eV) and at the resonance energy E_0 (931.2 eV).

techniques are also able to distinguish localized bonding contributions from more band-like features.

To decide on the possible non-planar interactions in the electronic structure, we report on polarization-dependent resonant photoemission profiles at the Cu2p absorption edge for BISCO single crystals recorded at 17 K and at 300 K (room temperature, RT). We give direct experimental evidence that mixed-atomic Sr, Bi, and O2p states do indeed exist, and contribute to the uppermost valence states and to the hole-doping mechanism. They are oriented perpendicular to the Cu–O plane and are linked to the apical oxygen atom (O_{api}). Applying polarization-dependent photo-excitation we are able to form conclusions on the 3D charge density distribution of the highest valence states and to distinguish the in-plane Cu–O contributions from those of the neighboring Sr-O plane via the $O_{api}(p_z)$ orbitals.

Experimental

Single crystals of double-layer optimum doped $Pb_{0,4}Bi_{1,6}Sr_{2,0}CaCu_2O_8$ ($T_c = 92$ K, $n_H \sim 0.16$) ((Pb, Bi)-2212-opt), of single-layer slightly underdoped $Pb_{0,6}Bi_{1,4}Sr_{1.5}La_{0.5}CuO_6$ ((Pb, Bi)-2201-ud) ($T_c = 24$ K, $n_H \sim 0.14$), and of heavily underdoped, not superconducting $Pb_{0,27}Bi_{1,6}Sr_{1.2}La_{0.8}CuO_6$ ((Pb, Bi)-2201-hud) ($n_H \sim 0.06$) were investigated. All of them were characterized by Laue diffraction, magnetic ac-susceptibility, and by energy dispersive fluorescence.

Photoemission spectroscopy (PES), resPES, and x-ray absorption (XAS) measurements were carried out at the BESSYII beamline U49/2-PGM2 [19–21]. Samples were cleaved in ultra high vacuum and transferred *in situ* to the cryostat. Constant initial state (CIS) data were recorded at a fixed initial state energy. XAS data of the selected initial states were deduced by summing over all resPES data to give partial integrated yield (pIY) spectra. These XAS-pIY data show the resonant contributions at the Cu2p edge, without inelastic features and just for the selected initial state energies.

Results and discussion

In figure 1(a) an overview resPES profile is presented for the double-layer ((Pb, Bi)-2212) BISCO at the Cu2p edge at RT. It is recorded by measuring several VB spectra using excitation energies between 925.5 eV and 964.5 eV, i.e. around the Cu2p absorption threshold. Two of these VB data, recorded before (927.5 eV) and at the resonance energy E_0 (931.2 eV) are depicted separately in figure 1(b). The resPES profile in figure 1 is displayed in a contour plot in which the obtained intensities are color-coded in a logarithmic scale (100 cps to 58 kps). The profile has been recorded in two separate runs and the data are stitched together at the black line. In this profile the PES lines of the Cu3d and O2p states (1) in the VB (at −4 eV), of the Sr4p (at −17 eV), and of the Bi5d (at −26 eV) levels appear as horizontal lines.

Our resPES data are discussed in terms of the Kramers–Heisenberg (KH) description [22]. The photo-excited electron (dipole matrix element M_1) rests in an intermediate state $\langle j|$ before it decays in a different channels matrix element (M_2). The resPES data of figure 1 represent the resulting intensity $I(i, \omega)$ for the individual initial states $\langle i|$, their energies E_i and

Table 1. The initial and final states observed for BISCO samples at the Cu2p resonance. One-, two-, and four-hole (1h, 2h, and 4 h) processes and spectator (S) processes occur. The indices refer to the decay path as displayed in figures 1 and 2.

Label	Initial state	Holes	Final state	Index
VB	$3d^9$	1h	$3d^8$	1
sat	$3d^84s^1$	1h	$3d^8$	2
		2h	$3d^7$	3
	$3d^9L4s^1$	P	$3d^9L4s^0$	
		S	$3d^7L4s^1$	4

the particular excitation energies $\hbar\omega$ around the threshold energy E_0. The intermediate state $\langle j|$ reflects all dynamic interactions of the photo-excited electrons with the VB and CB states during its lifetime $\hbar/\Gamma$.

$$I_{res}(i,\omega) \approx \sum_j \left| \frac{\langle f|\, M_2|j\rangle\, \langle j|\, M_1|i\rangle}{E_i - E_0 - \hbar\omega - i\Gamma_j} \right|^2 \quad (1)$$

This advanced technique enables us to follow the individual decay channels which originate from the KH intermediate state $\langle j|$ [22][3] (see next subsection). Thereby, at the Cu L_3 edge we monitor the variations of the VB states, of the $Cu3d^8$ satellite ($Cu3d^8$-sat), and of the individual Auger processes in detail. The resonant decay paths involve participator and spectator decays with 1h and (2h, 1e) final states, respectively. We have recently established this technique for the analysis of localized states in graphene [23] and in transparent conductive oxide materials [24–26].

In figure 1 the Cu-$L_3(L_2)$ resonance energy E_0 occurs at an excitation energy of 931.2 eV (951.8 eV). The observed spectroscopic features contain PES lines and participator decays with a 1 hole (1h) final state, as well as Auger decays with 2h or 4 h final states. The PES of the VB (at −4 eV, (1) in figure 1(a) and in table 1), of the Sr4p (at −17 eV) and the Bi5d (−26 eV) levels appear as horizontal lines in figure 1(a). We find a smoothly decaying intensity for all VB states above the resonance energy.

The $Cu3d^8$-sat (2) appears as a strong delta-like resonance (at $h\nu \sim 931.2$ eV, initial state energy ∼12.5 eV). It originates from a shake-up process which brings the $3d^9$ into a $3d^84s^1$ constellation (see also (2) in table 1). It is remarkable that the main intensity at the Cu2p resonance is in the $Cu3d^8$-sat. It shows a characteristic multiplet splitting (^1S, ^1G, and ^3F) which identifies the $Cu3d^8$ configuration. The splitting is noticeable but appears rather broad in our ((Pb, Bi)-2212) data in figure 1(b) with the VB spectrum at resonance. The intensity of the $Cu3d^8$-sat can be used as measure for the admixture in the ground state by comparing the intensities of the spectra before and at resonance. From the data shown in the VB panel in figure 1(b) we deduce that there is about a 50% admixture of the $Cu3d^84s^1$ state. Obviously, this state is very stable and upon resonant excitation it is populated preferentially, in agreement with [27]. This $3d^84s^1$ satellite decays as a participator into the $3d^8$ final state (2) and as a spectator into the $3d^7$ final state. The latter propagates at a constant kinetic energy of 918 eV under 45°, similar to the normal Cu-LMM Auger process (3).

In figure 2 we show resPES data of ((Pb, Bi)-2201) ($T_c = 24$ K). This represents a single-layer BISCO system and can be compared to the double-layer system depicted in figure 1. Here we show the data for excitation energies between 926 eV and 950.5 eV. The measurements were made at 17 K. This temperature is well below the T_c (24 K) of the sample. In these contour plots the color-coded intensities range between 10 cps and 11 kps; they are again displayed on a logarithmic scale. The corresponding resPES profiles of the double layer ((Pb, Bi)-2212) at the Cu2p edge in out-of-plane polarization show similar results when compared to the corresponding data (at RT) of the double-layer BISCO system (see figure 1). In figure 2 we directly compare the resPES profiles recorded in out-of-plane (figure 2(a)) and in-plane (figure 2(b)) polarization geometries, both recorded at 17 K. Again, the decay channels of the VB (1), of the $Cu3d^8$-sat (2), and of the Sr4p and Bi5d emissions, are marked for clarity. In both resPES profiles the resonance energy E_0 is at 931.2 eV (white vertical lines). The Sr4p and Bi5d PES channels show a weak but sharp resonance right at E_0.

In the following sections we discuss the details of the Cu-LMM Auger process and its polarization dependence, explain the formation of the double-spectator processes with a 4 h final state, and focus on the consequences for the electronic structure of the BISCO systems.

The Cu-LMM Auger intensity appears at 45°. It is very weak in the in-plane polarization (figure 2(b)) and strong in the out-of-plane polarization (figures 1 and 2(b)). In the polarization-dependent data with the out-of-plane configuration (figures 1(a) and 2(a)), the intensity of the Cu-LMM channel is readily observable and it starts directly at the main intensity of the $Cu3d^8$ satellite. The intensity of the LMM Auger is expected to be higher when excited by out-of-plane polarized light as it involves the $Cu3d(z^2)$ and $Cu3d(x^2 - y^2)$ orbitals which are oriented normal to the Cu–O plane.

One of the experimental highlights in our resPES study is the significant enhancement in intensity when the Cu-LMM line crosses the region of the Sr4p core levels at an initial state energy of ∼18.5 eV. In addition, there are some weaker resonant contributions of this Auger decay occurring at the Bi5d core levels at ∼25.5 eV and ∼28.5 eV initial state energies. According to the out-of-plane polarization used, the Cu-LMM Auger process must now involve the out-of-plane wave functions of copper and oxygen: the $Cu3d(z^2)$ or $3d(x^2 - y^2)$ and the $O_{api}(p_z)$ atomic states. The observed resonant enhancements then indicate that these perpendicular Cu–O states are able to mix with the large 5 s and 6 s wave functions of the Sr5s and Bi6s atoms, and they must contribute to a common valence state V(s) which becomes

[3] We use the KH formula which originally is suggested to describe pure atomic processes close to the threshold energy. We modify the description for solid state systems. We use the lifetime of the intermediate state -i Γ as the core hole is screened effectively due to the high carrier density in the valence band and its lifetime is no longer the rate-determining quantity. The sharp and at present resolution-limited excitations due to d-d excitations, magnons and charge transfer excitations seen in RIXS on open shell systems like cuprates further corroborate our view.

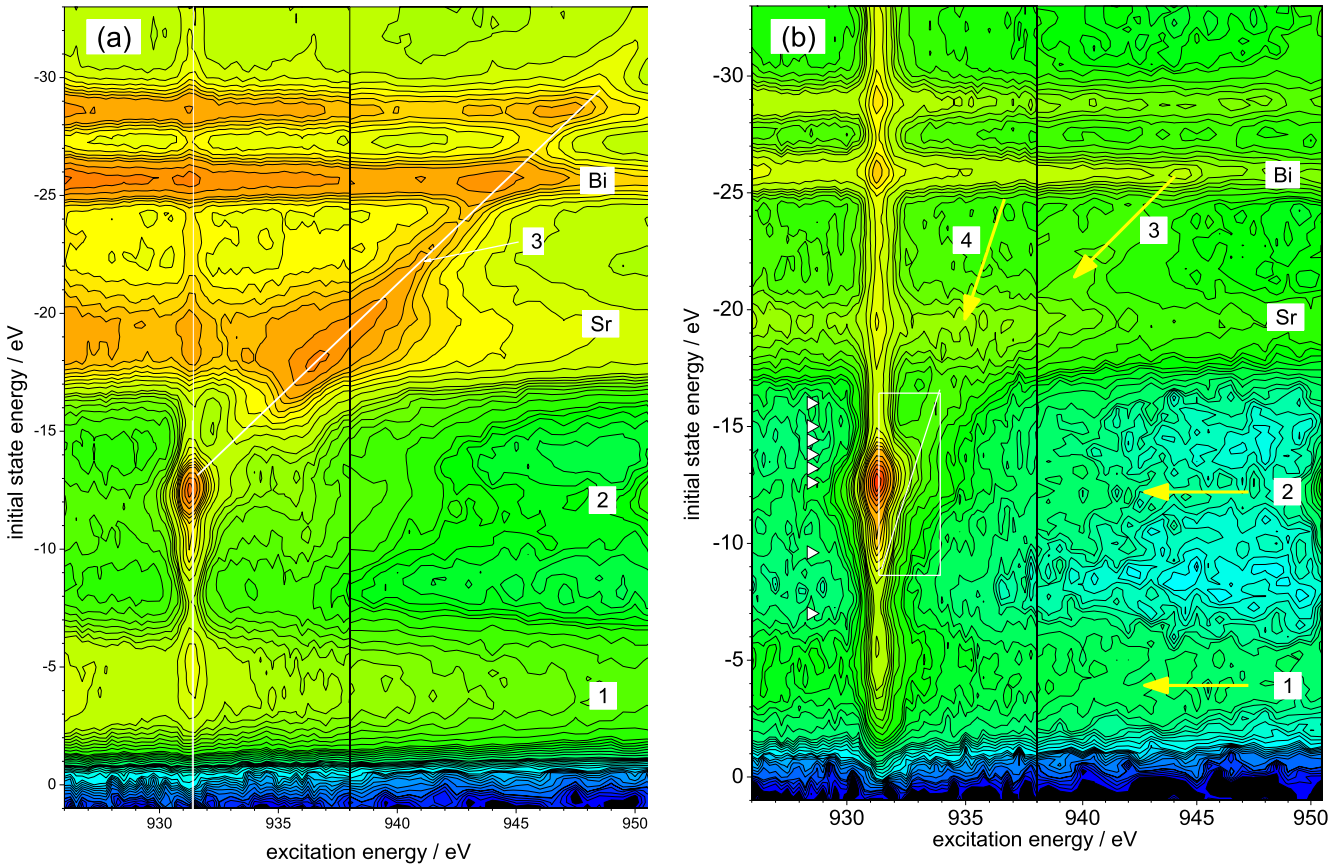

Figure 2. resPES profiles of ((Pb, Bi)-2201) around the Cu L_3 edge with out-of-plane (figure 2(a)) and in-plane (figure 2(b)) polarization, both recorded at 17 K. The data have been recorded in two separate runs and are stitched together at the black line. The PES lines of the Cu3d and O2p states in the VB (1), of the Sr4p (at −17 eV) and Bi5d (−26 eV) levels appear as horizontal lines. (2) indicates the position of the $Cu3d^8$ satellite. The 4h-Auger ((4), white line in the rectangular box in figure 2(b)) and the 2h-Cu-LMM ((3), thin white line in figure 2(b)) processes are marked. The yellow arrows in figure 2(b) indicate the directions of the individual decay processes.

involved in the Auger process. The hybridization of the Sr and the Bi states can be understood as the large spatial extension and low symmetry of the Sr5s and Bi6s wave functions facilitating a hybridization. These states are then able to mix into the Cu(4 s) and the O_{api} ($O2p_z$) states.

Consequently, it is straightforward to assign the observed enhancements to extended mixed-atomic valence states V(s) in an Auger process with a Cu2p-Cu3d-V(s) configuration of the Cu LMV process. The valence state V(s) must then contain contributions of in-plane and out-of-plane directed atomic orbitals which are represented by the terms $V^{\parallel}$ and $V^{\perp}$. Both are in essence composed by the 4 s, 5 s, and 6 s wave functions of Cu, Sr, and Bi, respectively:

$$V(s) = V^{\parallel} + V^{\perp} = V(\mathrm{Cu4s},\ \mathrm{Sr5s},\ \mathrm{Bi6s}).$$

The $V^{\perp}$ term also includes the out-of-plane wave functions of oxygen and copper: $O_{api}(p_z)$ and $Cu3d(z^2)/Cu3d(x^2 - y^2)$. This term creates a dipole moment perpendicular to the Cu–O plane which enhances the LMV(s) Auger. Based on its mixed-atomic configuration, a single-atomic description fails.

In the in-plane polarized data displayed in figure 2(b), the intensity of the Cu-LMV process (3) is much weaker and is barely observable. This gives a chance to study in more detail the role of the V(s) states within the Cu–O plane and without the contributions of the out-of-plane O_{api}, Sr, and Bi contributions. In fact, there is a different process (4) which clearly differs from the standard 2h Cu-LMM Auger behavior.

It does not follow a 45° slope but rather proceeds next to the $Cu3d^8$-sat with a slope of about 75° (bold white line, (4)). In our data the 4 h Auger signal arises at initial state energies ≈ 3 eV below the main $Cu3d^8$-sat emission, and it propagates along its wing on the right-hand side. Thereby, it causes the asymmetric shape of the $Cu3d^8$-sat and unravels the origin of this absorption feature, which is typical for the in-plane Cu L-edge XAS data of the BISCO systems (see below).

This is another of the most significant observations in our study, as there is no evidence for a distinct separate peak in the Cu L-edge absorption data. Here we benefit from our sophisticated experimental approach to resolve the absorption features for each initial state. This gives more detailed information than the commonly-used TEY-XAS data, which are integrating over all spectral features including inelastic processes. Instead, in our data we find a shoulder which propagates next to the Cu3d satellite feature (marked by the white line in figure 2(b)). The process (4) observed in figure 2(b) clearly differs from the standard 2h Auger behavior. This feature can be attributed to a process in which

double-spectator ($S^* + S^*$) Auger decays occur. They lead to a 4 h final state with a characteristic slope of about 75°.

Double-spectator (4 h) processes in BISCO

Deviations from the standard 2h Auger decay occur when localized (correlated) electrons are involved in the Auger decay [23, 26]. A characteristic of such 4 h processes is their enhanced kinetic energy (with respect to the common 2h Auger), which is due to the release of the correlation energy involved. The appearance of such 4 h processes gives direct evidence that the Auger electrons are emitted out of localized electronic states and not from extended band-like states. In our data the 4 h Auger proceeds with a slope of about 75° (white line, (4)) and the signal almost merges with the main $Cu3d^8$-sat emission. Consequently, the asymmetric shape of the $Cu3d^8$-sat is caused by this double-spectator decay rather than by a separate absorption state.

From the data in figure 2(b) we are able to determine the range in which the 4 h process shows up. We observe the characteristic features in the white rectangular region, which has a width of about 2 eV and a height of about 8 eV, in figure 2(b).

Multiple Auger processes such as ($S^* + S^*$) arise when the photo-excited electron becomes trapped in a band of localized states. (S^*: spectator; the * marks spectator processes in which the uppermost energy states contribute, and distinguishes it from those which involve only lower VB states.) This causes a significant change in the intermediate state: it increases the lifetime and thereby initiates the double-spectator process.

The 4 h final state can be understood to be caused by localized states which involve the Coulomb interaction due to a ligand-to-metal CT from the O2p ligands. Starting from the $3d^8$ configuration of the Cu-sat, these are the $3d^9L$ and the $3d^9L4s^1$ states, which lead to the appearance of the non-45° Auger contributions. Such Auger decays are not evident in the out-of-plane polarized data, and they are absent in CuO (not shown). They involve an in-plane ligand-to-metal CT state which enables a combined double-spectator Auger decay with a four-hole (4 h) final state [20, 21, 23–26]. Therefore, the in-plane CT within the O-Cu–O plane main absorption signal is not from the $3d^9$, $3d^8 4s$ configurations of the Cu ground state, but arises from the mixed-atomic $3d^9L4s^1$ state.

A characteristic of such double-spectator 4 h processes is their enhanced kinetic energy (with respect to the common 2h Auger process) which is due to the release of the correlation energy involved. Hence, their appearance is direct evidence for localized electronic states not involving band-like states. The localization is considered as weak and it may be caused by polaronic charge trapping or by polarization effects of the charge carriers within the V(s) band.

Combined Auger processes require that in the narrow band in which the photo-excited electron is temporarily accommodated, a second intermediate state is available. Such a situation occurs when at resonant excitation and in the time window of the first S^* spectator decay, simultaneously a second, combined decay becomes possible. This explains the high intensity of our data in figure 1 right at the Cu2p resonance. Consequently, the lifetime of the intermediate state now reflects the different localization. It is shorter for band-like states and longer for localized states. This is a unique method to learn about such lifetime variations resulting in participator or spectator processes.

For the Cu–O and BISCO systems, the consequences of the multiple Auger processes and their mechanisms will now be explained in more detail. Generally, Auger processes involve the lower VB states to fill the empty core hole levels caused by photo-excitation. At resonant excitation, they may form spectator decays (S) in which two valence holes are formed while the photo-excited electron remains in the CB states (2h, 1e). It is very important to note that resonant excitation also enables the uppermost valence/energy states of the V(s) to become involved in the Auger processes to enable the S^* processes, in particular.

Our assignment is confirmed by the corresponding data (not shown) recorded at the O1s absorption edge. There we find combined O1s-O2s-V(s) Auger processes, which again points to the localization of the carriers within the V(s) band. They involve an in-plane ligand-to-metal CT state which yields to a combined double-spectator Auger decay with a four-hole (4 h) final state [20, 21, 23–26]. For the in-plane CT within the O-Cu–O plane main absorption signal is not from the ground state $3d^9$, $3d^8 4s$ but from the mixed-atomic $3d^9L4s^1$ state.

Some more details about the mechanisms of the double-spectator process are displayed schematically in figure 3. In the right part we show a band scheme of the valence states with the lower VB and the upper V(s) band involved in the Auger processes. In that scheme we include the schemes of the single-spectator S and S^* which are the spectator processes of the lower and of the upper valence states created upon resonant excitation, respectively (right). For both parts, the direction of the increasing photon energy ($\hbar\omega$) is indicated. The red asterisk marks the energy value for resonant excitation. Please note that the axis of the excitation energy $\hbar\omega$ differs in the two sketches. The blue arrows symbolize the Auger decay processes S and S^*. The left part shows a schematic sketch to represent the resPES profiles of figure 2(b) indicated by the white rectangular region around the Cu-sat. In our resPES profiles the states next to the threshold energy E_0 originate from the narrow band formed by the V(s) states. The V(s) band has a width of ΔW and can be reached upon resonant excitation at threshold (red asterisks in figure 3). As this upper V(s) band is partially filled with electrons, these are available to become emitted as spectator electrons. The states in the V(s) band are localized by a correlation energy ΔE_c and therefore they form S^* processes which are then observed for excitation energies right above the resonance energy $E_0 + \Delta W$ (see figure 3, left). The width of the V(S) band is directly related with the experimental observed width of the double-spectator range.

The kinetic energy of the $S^* + S^*$ process is determined by the sum of the increase in photon energy and by the correlation energy ΔE_c released with the emitted electron. The

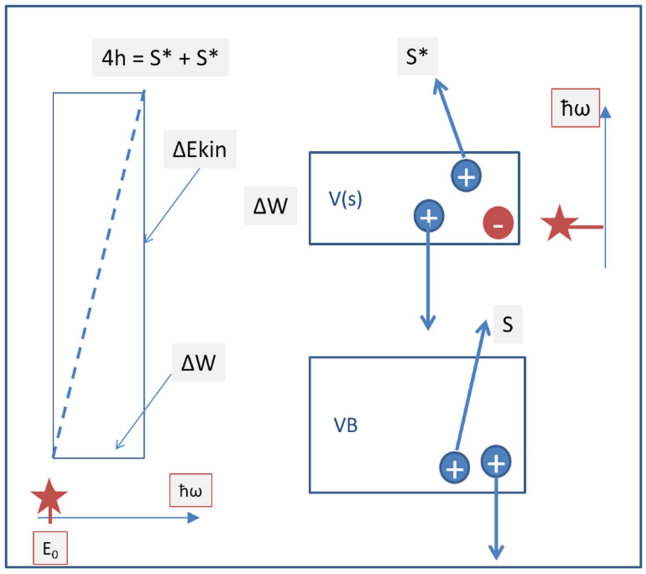

Figure 3. Sketch of the Auger processes originating out of the lower valence band (VB) and of the upper VB V(s) upon resonant excitation ($\hbar\omega$). S and S^* denote the spectator processes of the lower and upper valence states upon resonant excitation, respectively (right panel). Schematic representation of the 4 h ($S^* + S^*$) spectators of the upper (S^*) valence states (left panel). This left sketch indicates the region in which the 4 h process (dashed line) can be observed, as indicated by the rectangular box with a width of ΔW and a height of ΔE_{kin}.

quantities are comparable in their energy values, and a single S^* process would lead to a $\Delta E_{kin}/\Delta W$ ratio of about 2:1. For the 4 h ($S^* + S^*$) processes the increase in kinetic energy then is doubled, resulting in the slope of about 4:1 (75°). Such 4 h processes are typically observed in systems where the band width ΔW is small and the localization energy ΔE_c is weak [26]. This also requires that such processes appear only in the vicinity of the resonance energy E_0.

Two conclusions can be derived from our experiments. First, the data confirm the existence of the V(s) VB and its contribution to the in-plane electronic structure. Also, its location can be derived as it must be close to the Fermi energy (resonance energy). Further, there is an energy difference between the lower valence states (VB in figure 3) and the upper V(s) states, otherwise there would be an overlap and the localized states would not be observable at all. The S^* processes cause a higher kinetic energy of decay mechanisms associated with the latter. Second, we determine the localization energy of the trapped electrons from the width ΔW of the V(s) band, as this is the energy window in which the 4 h processes occur (see figure 3). The size of ΔW is the amount of energy transferred to the escaping Auger electrons, resulting in an additional gain in kinetic energy ΔE_{kin}. The value of about 2 eV is consistent with a weak correlation energy, which is expected for polaronic charge screening or by the polarization of the carriers in the partial filled V(s) band.

The fact that the in-plane Auger signals appear only close to the resonance energy E_0 indicates that the lifetime in the intermediate state Γ (see KH formula (1)) is rather large, and

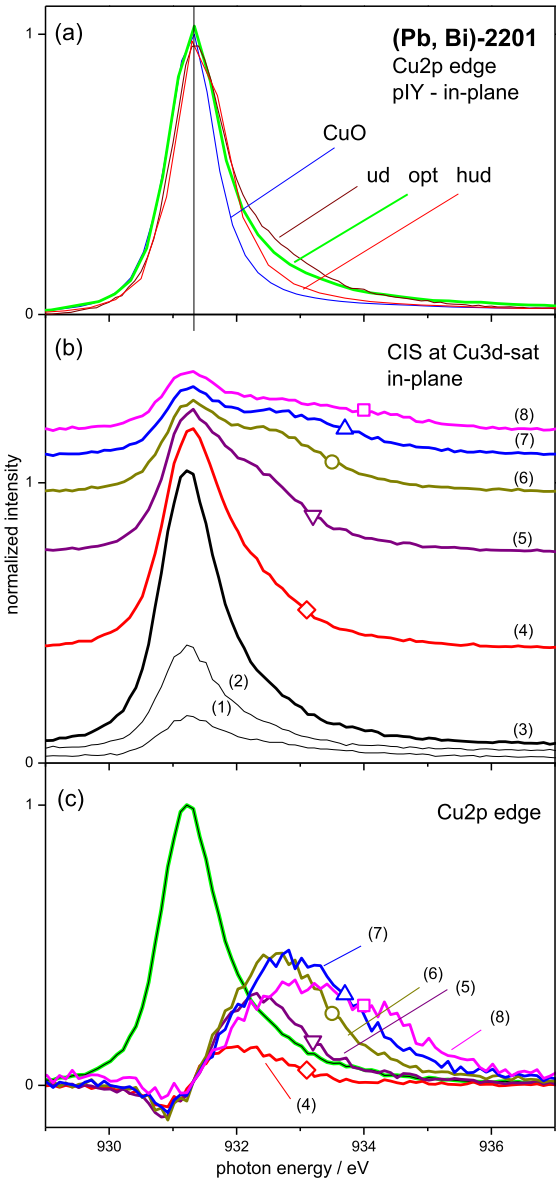

Figure 4. (a) The Cu2p-pIY absorption signal of ((Pb, Bi)-2201-ud), heavily underdoped, and non-superconducting ((Pb, Bi)-2201-hud). For comparison, the corresponding data of CuO and of ((Pb, Bi)-2212-opt) are also included. (b) CIS spectra as taken at various initial state energies along the Cu3d-sat (as marked by the white triangles in figure 2(b)). The shoulders in the CIS curves attributed to the 4h-Auger process are marked by ticks. They correspond to the intersection of the CIS data with the white line (4 h) in figure 2(b). There, the initial state energies of the CIS curves are marked by the small triangles. Here, the numbers indicate the sequence of the triangles, starting from the lowest initial state energy of −7 eV, which is outside of the rectangular box of figure 3 but is used as a reference for all CIS curves shown in figure 4(b). (c) The pIY (figure 4(a), opt) and the CIS at the Cu3d satellite (curve (3) in figure 4(b), normalized and plotted together: they coincide and form a single peak at about 931 eV; the difference curves of the CIS data in figure 4(b) with respect to curve (3) showing the Auger contributions of (4–8) enlarged by the normalization procedure.

this again points to the existence and contributions of localized states. The broadening of the main line is evident in our pIY-XAS data, which are shown in figure 4(a). Here we find the smallest width for the reference material CuO (mimicking

the anti-ferromagnetic (AF) phase). We understand in terms of the KH model that there the lifetime of the Cu2p resonance is very long. The investigated BISCO samples show a weak energy broadening with respect to the CuO data, which indicates that the lifetime τ of the intermediate state is reduced. This indicates an increase in covalent bonding between the oxygen ligands and the Cu atom. However, it should be mentioned that this increase is very weak and some localized charge density is still maintained as the lifetime broadening is rather weak.

This interpretation in terms of a lifetime broadening conflicts with the general interpretation, which assigns the asymmetric peak shape to a discrete absorption band at around 932.7 eV. Generally, the intensity of that shoulder is used as a measure of the doping concentration [e.g. 7, 9]. There are several arguments against that interpretation. The first reflects the fact that the shoulder is more pronounced in commonly-applied TEY data; the signal is much weaker in our pIY data. This indicates that low energy inelastic scattering processes contribute and may blur the TEY signal. Such disturbing processes can be avoided by recording the pIY data in which only the significant initial states of the valence regime are involved, and the true absorption profile becomes evident.

The second argument considers the individual CIS data taken around the $Cu3d^8$-sat emission of the investigated BISCO samples. Here it becomes evident that the additional features appear only at initial states above the Cu2p satellite peak (initial state energy $>$ 13 eV, curves 4–8 in figure 4(b)). In curves 1–4 there is no single static feature visible, as would be expected for a discrete absorption level. Instead, additional features appear only at initial state energies above 13 eV and show up right at the onset of the 4 h and 2h Auger processes (marked by the yellow arrows 4 and 3, respectively, in the resPES data in figure 2(b)). Furthermore, these additional features disperse in energy, and they do not appear at a fixed excitation energy. In figure 4(b) we analyze the resonance profiles of the 4 h double-spectator process (4) of figure 2(b) for individual initial state energies and display the CIS spectra obtained from the in-plane data as marked by the white triangles in figure 2(b). These individual curves allow us to follow the intensity variations for individual initial state energies, and with that they are more precise than the integrated pIY data. This allows detailed analysis of the energy shifts of the individual decay mechanisms. The position of the 4h-Auger process are marked by the open symbols in the curves. These contributions disperse under an angle of 67° in figure 2(b). They originate at the resonance energy E_0 and cause the asymmetric broadening next to the main line. This behavior again reflects the existence of the 4 h Auger emission. In addition, the CIS curves show contributions of the normal Auger process (marked by the yellow arrow 3 in figure 2(b)), which disperse under an angle of 45°. Finally, there is a participator contribution which appears at a constant initial state energy of around 12.5 eV (marked by the yellow arrow 2 in figure 2(b)).

In figure 4(c) we have plotted the difference curves of the corresponding CIS data, normalized to the Cu3d satellite intensity. Again, the contribution of the 4 h process is marked by the open symbols. With that procedure the dispersion of the two Auger contributions becomes more pronounced. The two Auger decays have a different dispersion and the resulting curve appears different for each individual initial state energy. It should be mentioned that the commonly-used TEY data integrate over these individual processes, and the above discussed detailed analysis is possible only in our resPES data. In addition, in figure 4(c) we compare the pIY signal (figure 4(a), opt) and the CIS spectrum 3 in figure 4(b). The close correspondence of these two different data underlines that the lifetime broadening at the Cu2p absorption edge is dominated by the lifetime of the Cu3d satellite. Any Auger contributions will cause a constant background in the pIY data but will not change the spectral width. Again, there is no indication of an additional absorption feature.

As a result of this analysis, our key conclusion is that the additional structures in the Cu2p absorption data arise from dispersing features associated with the 4-hole and the 2h-hole Auger processes. This result departs from the often-used interpretation as a doping feature as demonstrated in detail above. In particular, there is no evidence of an additional discrete absorption signal separated from E_0, as is often assumed in XAS-TEY data analysis [e.g. 7, 9]. The asymmetry of the Cu absorption signal definitely varies with doping. However, it is not an additional absorption band; it just reflects a change in the lifetime of the intermediate state. Our analysis further allows us to identify the 4 h S^* Auger process as the main decay process as a consequence of the increased lifetime.

V(s) in the electronic properties of BISCO

The V(s) model in which the uppermost valence states are integrated describes our experimental findings consistently. The V(s) band is formed in essence by the Cu4s, Bi5s, and Bi6s states as well as by the corresponding O2p levels. The two components for $V^{\perp}$ and $V^{||}$ differ in their degree of hybridization, which is stronger in the out-of-plane $V^{\perp}$ part, as well as by their localization, which is stronger in the $V^{||}$ contribution due to the ligand-to-metal CT. These results can be deduced within the KH picture via the differences in the lifetime of the corresponding intermediate states. The in-plane has a lower hybridization with the V(s) states. The photo-excited electron which populates the j-state has a longer lifetime and becomes trapped in the V(s) band, its charge being screened by polarization of the electrons populating the V(s) band. This results in a localized Auger decay causing the double-spectator process (4 h final state). The out-of-plane hybridization, on the other hand, is much stronger. Now V(s) is more band-like and it enables the 'normal' Cu-LMM process, albeit with the contributions of Sr5s and Bi6s states—which must be band-like.

Combining these experimental findings and the data of figure 4(a), we can deduce that in the Cu–O plane the charge density consists of two coexisting contributions, a localized fraction and a covalent fraction. The former comes from the CT. It is localized in energy by the Coulomb interaction as

well as in space by the charge separation from the oxygen ligand to the next neighbor Cu atom. This localization is independently witnessed by the combined 4 h Auger processes (figure 4(b)) and by the weak lifetime broadening of the KH intermediate states (figure 4(a)).

In total, the valence state is described by the out-of-plane and in-plane components $V = V^{\perp} + V^{||}$ with the respective atomic orbitals involved $V = \{Cu4s\ O2p^{\perp}\ Sr5s\ Bi6s\} + \{Cu4s\ O2p^{||}\}$. As a consequence of this common valence state, the charge density of the Cu4s state can become distributed towards the *c*-axis because of its $V^{\perp}$ component. It nicely describes the experimental finding as it creates a dipole moment perpendicular to the Cu–O plane which enhances the LMV mixed Auger.

Most remarkable is that such a common valence state enables the covalent charge density within the Cu–O plane to become modified via the interplay between the vertical $V^{\perp}$ component and the in-plane $V^{\parallel}$ contributions. Indeed, our observation offers a description of the electronic properties which opens a new approach to understanding the formation of the superconducting state [27] hitherto not considered.

Our data not only demonstrate that the shoulder in the Cu2p XAS data is due to a 4 h Auger process, but also suggest that this double-spectator process is related to the mechanisms of the doping.

The doping within the Cu–O plane generally is attributed to the shoulder in the TEY-XAS signal on the high energy side of the Cu2p resonance, as shown by many earlier studies [7, 9, 28–32]. Here we demonstrate that there is no extra peak arising but the shoulder is predominantly caused by the 4 h Auger process. There are two major consequences for the charge distribution by this novel assignment with the double-spectator process. First, the localized nature of the Auger electrons observed at the O1s and the Cu2p edges indicates that the localization must involve both the O2p and the Cu3d states. Second, at the Cu2p edge it implies that the doping process occurs via the $3d^8 4s^1$ configuration of the Cu3d^8-sat [33] rather than with the $3d^9$ ground state. We conclude that the doping occurs via the $3d^9L4s^1$ configuration and includes the ligand-to-metal CT within the O-Cu–O plane. This implies that the Coulomb interaction between the O2p ligand hole and the electron at the Cu site causes the localization and leads to a charge separation between the ligand hole and the electron at the Cu metal site. The ligand-to-metal charge transfer creates a hole density at the ligand site and the corresponding electron density is transferred into the V(s) state. This state is able to communicate via the O_{api} orbitals with the mostly covalent charge density in the neighboring Sr-O and Bi-O planes, based on the low symmetry of the Sr5s and Bi6s wave functions.

The electron density at the Cu site is also in the uppermost valence state $V^{||}$. The corresponding wave function of the $\langle j|$ state can then be described by $\langle j| = \{Cu2p^5\ O2s^2\ O2p^5\ Cu3d^9\ V^{||}(4\,s)^1\}^{+1}$. Here the stability of the Cu3d^{8}4s^1 configuration of the Cu3d^8-sat is taken into account and the term $V^{||}(4\,s)^1$ describes the valence state in which the 4 s electron is accommodated. In the KH picture this intermediate state for the in-plane process decays into an Auger process which involves combinations of spectator decays ($S^* + S^*$), and results in a 4 h final state based on the localized valence states in the term $3d^9LV^{||}$. The observed multiple 4 h ($S^* + S^*$) Auger processes indicate that the Coulomb interaction within the $3d^9L4s^1$ Cu configuration stabilizes some charge density of the hole at the ligand site, as mentioned above. This novel concept is deduced from our resPES data and suggests that such a 3D charge network exists in the cuprates.

We would like to mention that our study indicates that these newly observed features in the electronic structure are observed in both the BISCO (with n = 1 and n = 2) Cu–O planes. Furthermore, they do not depend on the temperatures of the samples and in particular are observed at RT and below T_c. This comparison leads us to conclude that the mechanisms described here reflect the intrinsic properties of the electronic structure in this class of cuprates. In some theoretical models, such contributions of localized states are represented by introducing repulsive U-pd parameters [34] or by using Wannier functions [16].

With these experimental confirmations and novel insights to the electronic properties, we call this interaction a dynamic charge fluctuation between the in-plane and out-of-plane hybridized orbitals. This relates only to the covalent part of the charge density. The more ionic charge separation process of the oxygen-to-Cu CT processes leads to a fixed charge distribution around the individual atoms. This part is stabilized by the Coulomb interaction and it reflects in particular the atomic positions around the Cu atom. Their tuning by strain and chemical substituents was discussed recently in [35].

A similar charge transfer and 3D mechanism has been reported in a recent study on 1212-Mo-cuprate compounds [36], a highly 3D cuprate system. In analogy we can state that our observation of the V(s) interaction in the almost 2D BISCO system must be even stronger in more 3D cuprate systems, and we suggest that our model is also applicable for other members of the cuprate family. In a further experiment in $YBa_2Cu_2O_{6+\delta}$, a perpendicular transient state with highly coherent transport resembling a superconducting state up to RT was created by excitation with mid-infrared optical pulses, tuned to the resonant frequency of O_{api} vibrations [15, 37, 38]. Again, this highlights the importance of modulated lattice and electronic properties in out-of-plane geometry [39].

Our description is also in agreement with a recent NMR study [40] in which it was demonstrated that the hole density at the O sites differs from the electron charge density in the Cu site. The latter was found to vary depending on the substituents such as Y or Hg, Tl, and Bi.

At this point we would like to reflect on the close relation of our data with previous theoretical models [16]. In a five-band model the interaction of the O_{api} has been described by the hopping integrals between the individual O2p$_z$, Cu3d(z^2) and Cu3d($x^2 - y^2$) orbitals on one hand, and Wannier-type wave functions on the other hand, in order to describe the covalent and the localized CT processes, respectively. Our data are directly related to such a description, particularly concerning the interaction of the O_{api} with the Cu3d orbitals.

However, the new information is in the participation of the Sr4s and Bi6s orbitals and in the direct evidence of the CT processes within and perpendicular to the Cu–O plane. In that, our findings are in line with theoretical models [14, 16].

Conclusions

Our resonant profiles at the Cu2p edge bear three main findings. First, our results relativize XAS-TEY data which are often used to analyze doping behavior [7, 9–13, 41]. The observed broadening reflects an Auger process associated with the $Cu3d^8$-sat. It is not due to the formation of a new electronic state [7] and [9] and hence cannot be used for a quantitative analysis of the doping concentration.

Second, the Cu2p resonance profile is dominated by the existence of two different Auger channels with a strong polarization of in-plane and out-of-plane geometries. It should be mentioned that the Auger processes which deliver such detailed information about dynamics in VB and CB states are observable only in resPES studies. They do not appear in RIXS studies as they are not Raman-active.

Both the in-plane and out-of-plane Auger processes point towards a dynamic charge balance between the O2p and the Cu states. It is controlled by the competing contributions of the localized charge density—stabilized by the Coulomb interaction—and of the covalent charge density fluctuations to fill the V(Cu4s) states.

The valence state in which the Cu4s electron is involved mediates its charge density, not only within the Cu–O plane but also in the bonding behavior along the *c*-axis. Both the Coulomb contributions by the ligand-to-metal CT and the hybridization of the Cu4s, Sr5s, and Bi6s wave functions bring novel additional information to the electronic interactions of the cuprates and their superconducting state. We expect that the detailed balance of the charge distribution also has an influence on the $Cu–O_{api}$ bond length which gives a direct relation to T_c [16]. The stronger the V(s) population, the stronger is the covalent bonding causing a shortening of the ($Cu–O_{api}$) bond.

Third, the two identified Auger processes can be consistently described in the context of the KH scenario by introducing a valence state, which is the lowest available state in the CB. This implies that any charge fluctuation within the Cu–O plane will also influence the perpendicular direction via the charge density of the V(s) state [14]. This is one of the main findings of our experiments as this coupling provides an additional channel for the destruction of the AF order by doping-induced charge fluctuations. On the other hand, the above sketched influence on the ($Cu–O_{api}$) bond is directly related with a reduction of the valence charge density within the Cu–O plane increasing the hole concentration. With this consequence our model confirms the requests for a 3D mechanism [1, 5, 15, 42] to explain the formation and stability range of the superconducting state in the cuprate family.

Finally, the doping process can also be described by a fluctuating charge distribution, based on our data. The charge spill-over between in-plane and out-of-plane atoms enables the description of a 3D order parameter which is necessary for the continuous phase transition to the superconducting state [1, 2, 39]. Doping does not cause a new state caused by O2p and Cu3d interaction. Rather, the ligand-to-metal CT creates a hole density at the ligand site and the corresponding electron density is transferred into the V(s) state. This inter-atomic valence state communicates via the O_{api} orbitals with the mostly covalent charge density in the neighboring Sr-O and Bi-O planes, based on the low symmetry of the Sr5s and Bi6s wave functions. Here we deduce this kind of 3D charge network in the highly 2D BiSr-cuprates from our resPES data of the BISCO system. The results presented here will be a challenge for the corresponding data on other cuprate systems and will further stimulate the development of multi-orbital concepts and 3D models of the superconducting state, as mentioned in the introduction.

Summary

The resPES data at the Cu2p absorption edge of single- and double-layer BISCO samples exhibit a strong polarization dependence at RT and at well below T_c. In a consistent description within the KH scenario, we conclude as follows.

1. The observed broadening at the Cu2p edge is due to a lifetime effect of the intermediate state when going from AF-coordinated CuO to the BISCO family.
2. Two different Auger processes are identified for in-plane and out-of-plane geometries.
3. The in-plane CT from O2p to Cu3d dominates, as indicated by the appearance of ($S^* + S^*$) multiple Auger processes, and indicates the charge localization by the Coulomb contribution.
4. The regular LMM process is observed out-of-plane. It arises from the $Cu3d^8$ satellite and it includes contributions from Bi6s and Sr5s states besides those of the O_{api} and the Cu4s.
5. The covalent contribution of the O-Cu interaction causes the strong polarization dependence via the common V(s) valence state.

The detailed analysis of in-plane and out-of-plane charge interactions is enabled by the orbital selectivity of our resPES data. It allows us to conclude on a dynamic charge balance between the Cu–O plane and the Sr-O_{api} plane via the 3D valence state V(4 s). This valence state V(s) is the lowest possible excitation at the Cu2p edge. Our data underline the limited applicability of the widely used 2D models and will contribute to improving the theoretical 3D models for the description of the doping mechanisms of the cuprate superconductors.

Acknowledgments

We appreciate delightful discussions with G Seibold and E Sigmund. We thank A Krapf (HU Berlin) for providing the

BISCO samples. The experimental assistance of G Beuckert, J Haeberle, and of the BESSY staff is appreciated. This work is supported by DFG (SCHM 745/31-1).

ORCID iDs

Christoph Janowitz https://orcid.org/0000-0002-8713-5201

References

[1] Bednorz J G and Müller K A 1986 *Z. Phys.* B **64** 189
Chakraverty B K 1981 *J. Phys.* **42** 1351
[2] Plakida N M 1995 *High-Temperature Superconductivity: Experiment and Theory* (Berlin; New York: Springer)
[3] Zhang F C and Rice T M 1988 *Phys. Rev.* B **37** 3759
Varma C M, Schmitt-Rink S and Abrahams E 1987 *Solid State Commun.* **62** 681
[4] Emery V J 1987 *Phys. Rev. Lett.* **58** 2794
Eskes H, Sawatzky G A and Feiner L F 1989 *Physica* C **160** 424
[5] Mermin N D and Wagner H 1966 *Phys. Rev. Lett.* **17** 1133
[6] Kosterlitz J M and Thouless D J 1973 *J. Phys. C: Solid State Phys.* **6** 1181
Berezinskii V L 1971 *Sov. Phys. JETP* **32** 493
Berezinskii V L 1972 *Sov. Phys. JETP* **34** 610
[7] Chen C T, Tjeng L H, Kwo J, Kao H L, Rudolf P, Sette F and Fleming R M 1992 *Phys. Rev. Lett.* **68** 2543
[8] Peets D C *et al* 2009 *Phys. Rev. Lett.* **103** 087402
[9] Schneider M, Unger R-S, Mitdank R, Müller R, Krapf A, Rogaschewski S, Dwelk H, Janowitz C and Manzke R 2005 *Phys. Rev.* B **72** 014504
[10] Peets D C, Hawthorn D G, Shen K M, Sawatzky G A, Liang R, Bonn D A and Hardy W N 2010 *Phys. Rev. Lett.* **105** 199702
[11] Liebsch A 2010 *Phys. Rev.* B **81** 235133
[12] Chen C-C, Sentef M, Kung Y F, Jia C J, Thomale R, Moritz B, Kampf A P and Devereaux T P 2013 *Phys. Rev.* B **87** 165144
[13] Brookes N B, Ghiringhelli G, Charvet A-M, Fujimori A, Kakeshita T, Eisaki H, Uchida S and Mizokawa T 2015 *Phys. Rev. Lett.* **115** 027002
[14] Andersen O K *et al* 1995 *J. Phys. Chem. Solids* **56** 1573
Andersen O K *et al* 1996 *J. Low Temp. Phys.* **105** 285
Pavarini E, Dasgupta I, Saha-Dasgupta T, Jepsen O and Andersen O K 2001 *Phys. Rev. Lett.* **87** 047003
[15] Hu W, Kaiser S, Nicoletti D, Hunt C R, Gierz I, Hoffmann M C, Le Tacon M, Loew T, Keimer B and Cavalieri A 2014 *Nat. Mater.* **13** 705
[16] Feiner L F, Grilli M and DiCastro C 1992 *Phys. Rev.* B **45** 10647
[17] Takahashi T, Matsuyama H, Katayama-Yoshida H, Okabe Y, Hosoya S, Seki K, Fujimoto H, Sato M and Inokuchi H 1988 *Nature* **334** 691
[18] Zanoni R, Chang Y, Tang M, Hwu Y, Onellion M, Margaritondo G, Morris P A, Bonner W A, Tarascon J M and Stoffel N G 1988 *Phys. Rev.* B **38** 11832
[19] Schmeißer D, Hoffmann P and Beuckert G 2005 *Materials for Information Technology* (*Engineering Materials and Processes*) ed E Zschech *et al* (London: Springer) p 449
[20] Richter M, Friedrich D and Schmeißer D 2012 *Bionanoscience* **2** 59
[21] Michling M and Schmeißer D 2012 *IOP Conf. Ser.: Mater. Sci. Eng.* **34** 012002
[22] Glatzel P, Sikora M and Fernandez-Garcia M 2009 *Eur. Phys. J.-Spec. Top.* **169** 207–14
Kotani A 2005 *Eur. Phys. J.* B **47** 3–27
[23] Richter M, Starke U and Schmeißer D 2014 *J. Electron Spectrosc. Relat. Phenom.* **192** 1
[24] Schmidt S and Schmeißer D 2012 *Solid State Ionics* **225** 737
Richter M and Schmeißer D 2013 *Appl. Phys. Lett.* **102** 253904
[25] Haeberle J, Richter M, Galazka Z, Janowitz C and Schmeißer D 2014 *Thin Solid Films* **555** 53
[26] Schmeißer D, Haeberle J, Richter M and Brazda P 2015 *Nucl. Instrum. Methods Phys. Res.* B **364** 127–31
[27] Makarov I A, Shneyder E I, Kozlov P A and Ovchinnikov S G 2016 *J. Supercond. Nov. Magn.* **29** 1063
[28] Ronay M, Santoni A, Schrott A G, Terminello L J, Rowalczyk S P and Himpsel F J 1991 *Solid State Commun.* **77** 699
[29] Merrien M, Studer A, Michel C, Srivastava P, Sekhar B R, Saini N L, Garg K B and Tourillon G 1993 *J. Phys. Chem. Solids* **54** 499
[30] Pham A Q, Studer F, Merrien N, Maignan A, Michel C and Raveau B 1993 *Phys. Rev.* B **48** 1249
[31] Ghigna P, Spinolo G, Flor G and Morgante N 1998 *Phys. Rev.* B **57** 13426
[32] Karppinen M, Kotiranta M, Nakane T, Yamauchi H, Chang S C, Liu R S and Chen J M 2003 *Phys. Rev.* B **67** 134522
[33] Iwan M, Himpsel F J and Eastman D E 1979 *Phys. Rev. Lett.* **43** 1829
Chiang T-C and Eastman D E 1980 *Phys. Rev.* B **21** 5749
[34] McMahan A K, Annett J F and Martin R M 1990 *Phys. Rev.* B **42** 6268
Hybertsen M S, Stechel E B, Foulkes W M C and Schlüter M 1992 *Phys. Rev.* B **45** 10032
[35] Yee C-H and Kotliar G 2014 *Phys. Rev.* B **89** 094517
[36] Marik S, Labrugere C, Toulemonde O, Morán E and Alario-Franco M A 2015 *Dalton Trans.* **44** 10795
[37] Kaiser S *et al Phys. Rev.* B **89** 1845162014
[38] Fink J 2015 *Physik J.* **3** 18
[39] Janowitz C, Seidel U, Unger R-S, Krapf A, Manzke R, Gavrichkov V A and Ovchinnikov S G 2004 *JETP Lett.* **80** 819
[40] Rybicki D, Jurkutat M, Reichardt S, Kapusta C and Haase J 2016 *Nat. Commun.* **7** 11413
[41] Phillips P and Jarrell M 2010 *Phys. Rev. Lett.* **105** 199701
[42] Friedel J 1975 *J. Physique Lett.* **36** L-279